Journal of Materials Chemistry C

PAPER

View Article Online
View Journal | View Issue

Cite this: J. Mater. Chem. C, 2018, 6, 4273

Excess axial electrostatic repulsion as a criterion for pentagonal bipyramidal Dy^{III} single-ion magnets with high U_{eff} and T_B†

Zhijie Jiang,‡ Lin Sun,‡ Qi Yang, Bing Yin, * Hongshan Ke, Jing Han, Qing Wei, Gang Xie and Sanping Chen *

Received 22nd January 2018,
Accepted 13th March 2018

DOI: 10.1039/c8tc00353j

rsc.li/materials-c

In this work, a large excess of electrostatic repulsion, arising from the axial ligands, over that from the equatorial ligands is taken as the design strategy for high performance pentagonal bipyramidal (PBP) Dy^{III} single-ion magnets (SIMs). In this strategy, two PBP Dy^{III}-SIMs (**1** and **2**) [Dy(bbpen-CH_3)X] (X = Cl, **1**; Br, **2**; H_2bbpen = *N*,*N*′-bis(2-hydroxybenzyl)-*N*,*N*′-bis(2-methylpyridyl)ethylenediamine) were synthesized and structurally characterized on the basis of a highly symmetrical ligand H_2bbpen-CH_3 in which an electron-donating group (–CH_3) was installed to favor the conformation necessary for the axial oxygen atom coordinating to Dy^{III}. Dynamic magnetic measurements verify the value of our design strategy since complex **2** exhibits high performance with large U_{eff} (above 1000 K) and a high magnetic hysteresis temperature (15 K). *Ab initio* calculations further verified the importance of the high excess of axial interaction which eventually leads to the special electronic structure possessing the desired magnetic properties. The search for excessive axial repulsion is not incompatible with the strategy based on local symmetry around the central ion since various high-performance PBP Dy^{III}-SIMs of both clearly distorted and nearly ideal geometries successfully acquire such a kind of excess. Apparently this study presents an alternative to the designing strategy for promising SIMs.

Introduction

Slow relaxation of magnetization in bistable magnetic molecules, leading to effective magnetization blocking, is widely accepted as the origin of single-molecule magnets (SMMs),[1] which have great application potential in various fields, *e.g.*, quantum computing[2] spin-based electronics[3] and high-density storage of information.[4] A monometallic SMM, which is also termed a single-ion magnet (SIM) in which only one central metal ion exists, is a concise target suitable for the studies digging into the fundamental comprehension of the SMM properties.[5] This is because not only is the intermolecular interaction usually negligible in SIMs but also many recent breakthroughs in this field arise from SIM systems. Thus, the deep comprehension of SIM systems will not only increase the knowledge of molecular magnets but also promote the ultimate application of SMMs in real life.

In the recent progress, Dy^{III}-SIMs of pentagonal bipyramidal (PBP) geometry made important contributions.[5c–g] The first reports of SIMs that possess a barrier for the reversal of magnetization (U_{eff}) over 1000 K[5c] and blocking temperatures (T_B) around 20 K[5d] both belong to this group of the complex. Actually, the highest U_{eff} of PBP Dy^{III}-SIMs is 1837 K,[5e] which still keeps the current record among all the SIMs.

These high-performance PBP Dy^{III}-SIMs are usually deemed to arise from the possible high local symmetry of the Dy^{III} ion since the coordination geometries of some of them are verified to be close to a D_{5h} point group. However, if all the reported PBP Dy^{III}-SIMs are subjected to detailed continuous shape measurements (CShM), their SMM properties are not monotonously related to their degree of closeness to the perfect PBP geometry (Fig. S23, ESI†). An even larger puzzle indeed exists because the coordination geometries of some high-performance SIMs are actually different from the perfect PBP geometry when compared with those of similar structures but inferior SMM properties.[6]

For Dy^{III}-SIMs, the high axiality of all the Kramers doublets (KDs), especially the ground one, and a high degree of the co-linearity of the magnetic easy axis of various KDs could

Key Laboratory of Synthetic and Natural Functional Molecule Chemistry of Ministry of Education, College of Chemistry and Materials Science Northwest University Institution, Xi'an 710069, P. R. China. E-mail: rayinyin@nwu.edu.cn, sanpingchen@126.com

† Electronic supplementary information (ESI) available: Structure, magnetism, *ab initio* calculation, magnetic interaction analysis, Fig. S1–S32, Tables S1–S8, and the crystal information files of complexes **1** and **2**. CCDC 1583474 (**1**) and 1583475 (**2**). For ESI and crystallographic data in CIF or other electronic format see DOI: 10.1039/c8tc00353j

‡ These authors contributed equally to this work.

effectively suppress the unwanted fast relaxation, *e.g.*, quantum tunneling of magnetization (QTM) and the direct process.[7] Under these circumstances, large crystal field splitting will provide high U_{eff} that eventually leads to long relaxation time and high T_B for SMMs.[7] The KDs of the Dy^{III}-SIMs could be well described as the combinations of the components of the ground $^6H_{15/2}$ multiplet of Dy^{III}, *i.e.*, $|m\rangle$ where m ranges from $-15/2$ to $+15/2$.[7] In this approximation, the perfect axiality, *i.e.*, the ideal SIM, would be achieved if each KD consists of only one fixed $|m\rangle$ in a manner where the larger the absolute value of m, the lower the energy of the KD.[8]

In the ideal PBP geometry of D_{5h} symmetry, only axial components of the crystal field Hamiltonian exist and they will make KDs the desired composition. Thus, ensuring perfect axiality from high local symmetry should root in its capability to achieve a special composition of the KDs. However, when D_{5h} symmetry is actually unavailable for distorted PBP Dy^{III} complexes, is there any other driving force toward the special compositions of the KDs?

For the Dy^{III} ion, the electron density of the pure $|\pm15/2\rangle$ components is of oblate shape.[9] Therefore, the stronger the stabilization of this aspherical electron density is, the larger the contribution of the $|\pm15/2\rangle$ component in the ground KD, *i.e.*, stronger axiality, will be. In order to stabilize such oblate electron density, the electrostatic repulsion from the equatorial ligands should be smaller than that from the axial ligands as much as possible. In this way, distorted PBP Dy^{III} complexes, which are although apparently different from D_{5h} symmetry, could still be expected to have good SIM properties if a large difference between the interactions from the axial ligands and those from the equatorial ligands exists. That is to say, the key is the consistency between the oblate electron density of Dy^{III} and the electrostatic repulsions from the surrounding ligands.[6a]

Therefore, for the first time in this current work, a large difference between axial and equatorial electrostatic repulsions is considered as the design strategy, leading to the successful synthesis of two mononuclear Dy^{III} compounds of the local PBP geometry. Their magnetic properties are promising as the highest U_{eff} exceeds 1000 K and the magnetic hysteresis loop exists up to 15 K.

Experimental

Materials and measurements

All commercial reagents and solvents were purchased from Aldrich, Adamas and TCI. ^{1}H-NMR spectra were recorded on a Bruker AV-400 or AV-100 spectrometer. Chemical shifts (δ) reported in parts per million (ppm) are referenced relative to the residual solvent peak in the NMR solvent ($CDCl_3$: δ 7.26 ($CHCl_3$)). Data are represented as follows: chemical shift, multiplicity (s = singlet, d = doublet, t = triplet, q = quartet, m = multiplet), integration, and coupling constants in Hertz (Hz). The phase purity of the bulk samples was confirmed by powder X-ray diffraction (PXRD) measurements executed on a Rigaku RU200 diffractometer at 60 kV, 300 mA, and Cu Kα radiation (l = 1.5406 Å),

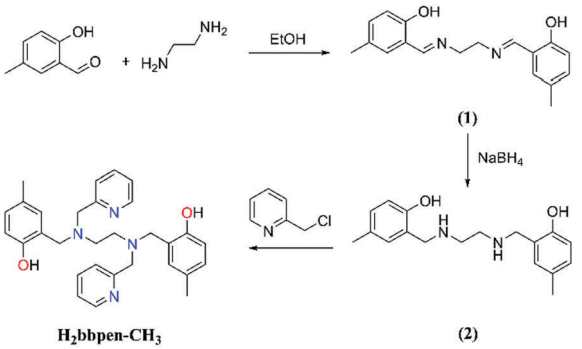

Scheme 1 Synthesis of the H_2bbpen-CH_3 ligand.

with a scan speed of 51 min^{-1} and a step size of 0.02° in 2θ. Magnetic measurements were performed in the temperature range of 2.0–300 K under 0 Oe, using a Quantum Design MPMS-XL-7 SQUID magnetometer on polycrystalline samples. The diamagnetic corrections for the complexes were estimated using Pascal's constants. Alternating current (ac) susceptibility experiments were performed using an oscillating ac field of 0 Oe at ac frequencies ranging from 0.1 or 1.0 to 1000 Hz. The magnetization was measured in the field range of 0–70 000 Oe (Scheme 1).

Synthesis

Synthesis of the H_2bbpen-CH_3 ligand. Ethylenediamine (3.85 g, 64 mmol) was added to a solution of 5-methylsalicylaldehyde (16.3 g, 120 mmol) in ethanol (85 mL). The reaction mixture was stirred at room temperature until the 5-methylsalicylaldehyde was consumed. A yellow precipitate was filtered off and dried *in vacuo* to obtain (**1**) as a yellow powder (16.7 g, 94% yield).

Sodium borohydride (5.1 g, 135 mmol) was added to a stirred suspension of (1) (16.0 g, 54 mmol) in 200 mL ethanol in three batches. The mixture was stirred for 2 hours, and hydrochloric acid (150 mL, 1.0 mol L^{-1}) was added dropwise. A white precipitate was filtered off and washed with water (3 × 10 mL) and ethanol (3 × 10 mL), and then dried *in vacuo* to give (**2**) as a white power (13.9 g, 86% yield).

A suspension of (2) (3.0 g, 10.0 mmol) was treated with NaOH (20 mL, 1.0 mol L^{-1}) and stirred until the mixture changed into a clear solution. 2-(Chloromethyl)-pyridine hydrochloride (previously neutralized with NaOH (25 mL, 1.0 mol L^{-1})) (4.1 g, 25 mmol) was added, and the reaction mixture was heated at 85 °C for 3 h. After cooling a white precipitate was filtered off and washed with water (3 × 5 mL) and cold ethanol (3 × 5 mL), and then dried *in vacuo* to give (**3**) as a white power (1.7 g, 35% yield).

^{1}H NMR (400 MHz, $CDCl_3$): δ 10.56 (s, 2H), 8.55 (d, J = 4.3 Hz, 2H), 7.61 (td, J = 7.7, 1.7 Hz, 2H), 7.16 (dd, J = 11.1, 6.4 Hz, 4H), 6.94 (dd, J = 8.1, 1.5 Hz, 2H), 6.7–6.62 (m, 4H), 3.73 (s, 4H), 3.64 (s, 4H), 2.73 (s, 4H), 2.21 (s, 6H).

Synthesis of [Dy(bbpen-CH_3)Cl] (1). A suspension of $DyCl_3 \cdot 6H_2O$ (37 mg, 0.1 mmol) and H_2bbpen-CH_3 (48.3 mg, 0.1 mmol) in EtOH (5.0 mL) was treated. After stirring for 15 min, the resulting mixture was immediately filtrated, and the filtrate was

left to stand at room temperature for slow evaporation. Colourless blocky crystals were gathered after three days in a yield of 68% (based on Dy^{III} salts). Elem. anal. calcd: C, 53.10; H, 4.75; N, 8.26%. Found: C, 53.01; H, 4.73; N, 8.25%.

Synthesis of [Dy(bbpen-CH_3)Br] (2). To a solution of H_2bbpen-CH_3 (48.3 mg, 0.1 mmol) in acetonitrile (6 mL) triethylamine (0.2 mmol) was added. After stirring for half an hour, the anhydrous $DyBr_3$ (40 mg, 0.1 mmol) solid was added, which was sealed in a 15 mL Teflon-lined stainless container and kept at 75 °C for three days, and then cooled to ambient temperature at a rate of 5 °C h^{-1}. Colorless block crystals were formed with a yield of 37% (based on Dy^{III} salts). Elem. anal. calcd: C, 49.84; H, 4.46; N, 7.75%. Found: C, 49.79; H, 4.42; N, 7.71%.

X-ray single-crystal diffraction analysis

Single-crystal X-ray data for complexes **1** and **2** were measured at room temperature on a Bruker Smart Apex CCD diffractometer with graphite-monochromatized MoKα radiation (l = 0.71073 Å) by using a ω and φ scan mode. Cell determination and data reduction were processed using the SAINT processing program.[13a] The absorption correction based on multiscan was applied in SADABS.[13b] By using Olex2,[14] the structures were solved by direct methods with SHELXS and refined by full-matrix least-squares techniques against F2 by using SHELXL-2014 programs.[15] All nonhydrogen atoms were refined anisotropically. All hydrogen atoms were placed in calculated positions and refined isotropically. The crystal data and structure refinement parameters are summarized in Tables S7 and S8, ESI,† whereas selected bond lengths and angles for complexes **1** and **2** are listed in Table S9 (ESI†).

Computational details

Multi-configurational *ab initio* calculations, including spin–orbit coupling (SOC), were performed on the experimental structures of complexes **1**, **1′**, **2**, **2′** (**1′** = [Dy(bbpen)Cl]), (**2′** = [Dy(bbpen)Br]), and **3** (**3**; $[Dy(O^tBu)_2(py)_5][BPh_4]$ possessing the highest U_{eff} among the PBP Dy^{III}-SIMs) to explore their magnetic anisotropy. This calculation consists of two steps:[16] (1) a set of SOC-free states, that is, spin eigenstates, are obtained by the CASSCF[17a] method and (2) the low-lying SOC states, that is, Kramers doublets (KD), herein, are obtained by state interaction,[16] that is, diagonalizing the SOC matrix in the space spanned by the spin eigenstates from the first step. All calculations were carried out using the MOLCAS 8.0 program.[17b] In the CASSCF step, the active space consisted of 9 electrons in 7 orbitals and all the spin eigenstates of 21 sextets, 224 quartets, and 490 doublets were included. In the subsequent state interaction, due to hardware limitations, only 21 sextets, 128 quartets and 98 doublet states were mixed by the RASSI-SO module.[17c] The ANO-RCC basis sets[17d,e] were used. The extraction procedure according to Chibotaru *et al.* was performed to obtain the g-tensors and transition magnetic moments of low-lying KDs with the SINGLE ANISO module.[18]

Results and discussion

Synthetic aspects

The electron-donating group $-CH_3$, at the 4-position of the phenol rings, is introduced in the H_2bbpen ligand to increase the electron density of the axial atoms coordinated to Dy^{III}. The reaction of the H_2bbpen-CH_3 ligand with DyX_3 (X = Cl, **1**; Br, **2**) in a 1 : 1 molar ratio gave two target complexes with the general formula [Dy(bbpen-CH_3)Cl] (**1**) and [Dy(bbpen-CH_3)Br] (**2**) by different reaction routes: slow evaporation and solvothermal synthesis, respectively (Fig. 1).

Crystal structures

Both complexes **1** and **2** crystallize in the monoclinic $P2_1/n$ space group without any crystallographic solvent molecules (Fig. S3, S4 and Table S1, ESI†). The CShM[7] results indicate that the $\{DyO_2N_4X\}$ cores of **1** and **2** are closest to the PBP geometry among all the ideal seven-coordinate geometries with the distortion of **2** (2.111) larger than that of **1** (1.824) (Table S3, ESI†). Two negatively charged phenol O atoms coordinate to Dy^{III} ions in the axial direction with the Dy–O distance in **2** (2.141 Å) shorter than that in **1** (2.155 Å). The O–Dy–O angles of **1** (158.070) and **2** (159.400) are close to each other but clearly deviate from 180°. The five equatorial coordination sites are occupied by four N atoms and one Cl for **1** or Br for **2** through the long average Dy–N distances (2.586 Å for **2** and 2.591 Å for **1**) and an even longer Dy1–Br1 (Dy1–Cl1) bond length of 2.852 Å in **2** (2.682 Å in **1**) (Table S2, ESI†). The Dy^{III} centers are isolated from each other by the bulky ligands: the closest distances of $Dy^{III}\cdots Dy^{III}$ ions are 8.479 Å for **1** and 8.470 Å for **2** (Fig. S5, S6 and Table S5, ESI†). To foster further learning about intermolecular interactions in our system, the two-dimensional (2D)-fingerprint of crystals and the associated Hirshfeld surfaces were employed. Based on the analysis of Hirshfeld surfaces, the weak intermolecular interactions of the neighboring molecules

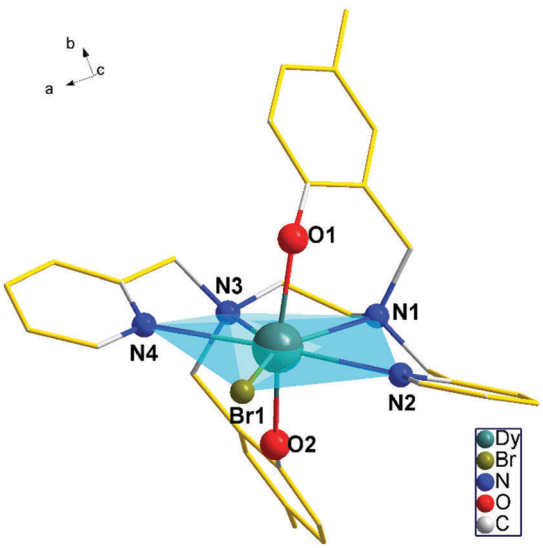

Fig. 1 Molecular structure of complex **2**. The equatorial plane of the pentagonal bipyramidal coordination sphere is highlighted.

are mainly H···H (**1**, 63.0%; **2**, 62.6%), C···H (19.9%, 10.6%), Cl···H (7.4%, 8.0%), O···H (5.8%, both **1** and **2**), C···C (2.1%, both **1** and **2**), and N···H (1.5%, 1.4%) (Fig. S7 and S8, ESI†).

Magnetic properties

At room temperature, the $\chi_m T$ values for **1** and **2** are 13.85 and 13.82 $cm^3\ K\ mol^{-1}$, respectively, lower than that expected for a free Dy^{III} ion (14.17 $cm^3\ K\ mol^{-1}$) due to the splitting of the $^6H_{15/2}$ ground multiplet (Fig. S9, ESI†). The non-superposition of the *M versus H*/*T* data on a single master curve suggests the presence of significant magnetic anisotropy and/or low-lying excited states (Fig. S10, ESI†). The maximum for χ_m'' (1000 Hz) appears at 55 K and 62 K for complexes **1** and **2** in zero dc field, respectively, showing the strong frequency and temperature dependence (Fig. 2, 3 and Fig. S11–S14, ESI†). Compared with Tong's work, the maximum peaks appear at higher temperatures with lower ac frequencies (50 K/60 K with 1488 Hz for **1**′/**2**′), implying the improvement of the SMM properties of our complexes.

For both complexes, the characteristic relaxation times are extracted using an extended Debye model (Fig. S18–S21, ESI†). The relaxation times τ extracted from the χ_m'' peaks for complexes **1** and **2** at selected temperatures under 0 Oe and 2000 Oe. In order to further verify the domination of the Orbach process at high temperature, relaxation time *vs.* temperature is plotted in the log–log scale (Fig. S22, ESI†), whose slope indicates that the Raman exponent is, respectively, $n = 12$ for complex **1** and $n = 18$ for complex **2**. The anomalously large Raman exponents ($n \gg 9$)[10,11] exclude the possibility of the presence of the Raman process in the high-temperature range, suggesting that the Orbach one is dominant. The relaxation times for complexes **1** and **2** at high temperatures obey the Arrhenius law ($\tau = \tau_0 \exp(U_{eff}/kT)$) with an effective energy barrier for relaxation $U_{eff}/k = 723$ K (502 cm^{-1}) and $\tau_0 = 2.36 \times 10^{-10}$ s for complex **1** and $U_{eff}/k = 1162$ K (808 cm^{-1}) and $\tau_0 = 1.02 \times 10^{-12}$ s for complex **2**.

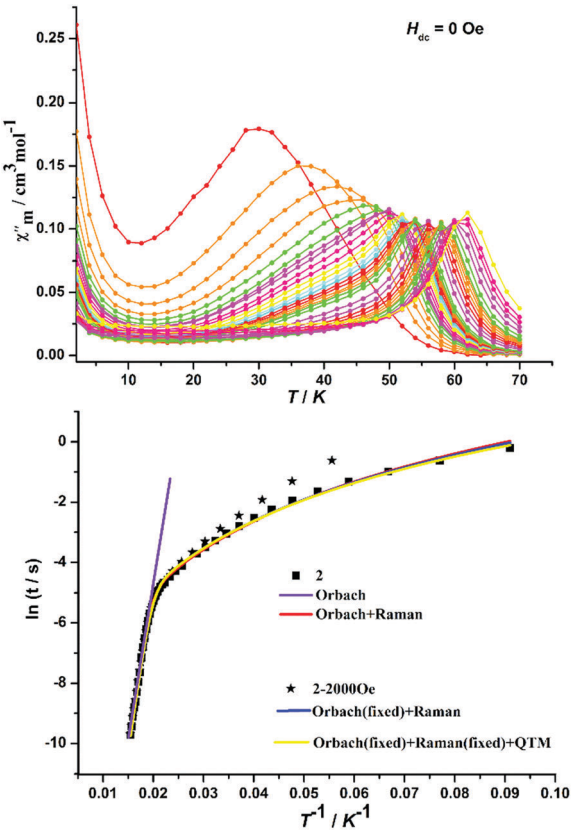

Fig. 3 Temperature dependence of the out-of-phase in zero dc field (up) and magnetic relaxation (down) for complex **2**.

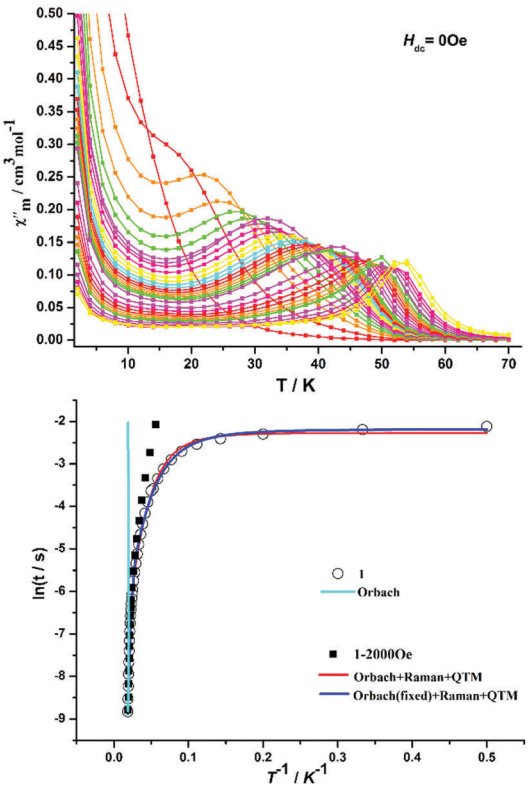

Fig. 2 Temperature dependence of the out-of-phase in zero dc field (up) and magnetic relaxation (down) for complex **1**.

For the relaxation time products under 0 Oe, the direct process can be neglected. In the low-temperature range, the Raman process still plays an important role in the relaxation times. In addition, the $\ln(\tau)$ *versus* $1/T$ plots for complexes **1** and **2** present some curvature (Fig. 2 and 3), indicating that the dynamics cannot be properly modeled assuming a simple Orbach mechanism. Therefore, the total relaxation rates mainly retain the Orbach process, Raman process, and QTM process, using the following equation (eqn (1)):

$$\tau^{-1} = {\tau_{QTM}}^{-1} + CT^n + {\tau_0}^{-1} \exp(-U_{eff}/kT) \quad (1)$$

where τ is the inverse of the ac frequency, T is the temperature of the maximum in the ac signal, U_{eff} is the effective energy barrier, and k is Boltzmann's constant. τ_{QTM}, C, and τ_0 are the fitting parameters of the different relaxation mechanisms.

In the absence of a static field, the independence of the relaxation time at low temperatures for complex **1** is indicative of a QTM relaxation process. The fit in the temperature range

T = 2–54 K for complex **1** by eqn (1) resulted in τ_{QTM} = 0.11 s, n = 2.97, $C = 4.60 \times 10^{-3}$ s^{-1} K$^{-2.97}$, $\tau_0 = 2.36 \times 10^{-10}$ s, and an effective energy barrier of U_{eff}/k = 723 K (502 cm^{-1}) (see ESI† for fitting details). The non-independence of the relaxation time at low temperatures for complex **2** indicates the absence of a QTM relaxation process. The fit in the temperature range T = 11–65 K for complex **1** by eqn (2) resulted in 3.15, $C = 5.35 \times 10^{-4}$ s^{-1} K$^{-3.15}$, $\tau_0 = 1.02 \times 10^{-12}$ s, and an effective energy barrier of U_{eff}/k = 1162 K (808 cm^{-1}) (see ESI† for fitting details).

$$\tau^{-1} = CT^n + \tau_0^{-1} \exp(-U_{eff}/kT) \quad (2)$$

T_{IRREV}, which is the point where the field-cooled (FC) and zero-field cooled (ZFC) susceptibilities diverge, is found at 12.1 K for complex **2** (Fig. 4), which clearly outweighs the value of complex **2′** (9.5 K). Magnetic hysteresis (Fig. 4) loops are clearly open at zero field up to 15 K for complex **2** (14 K for complex **2′**) at an average sweep rate of 0.02 T s^{-1} (time for a full cycle). For most SMMs T_B and T_{IRREV} are very similar, and observed differences have been assigned to a distribution of relaxation times.[12]

Either from the aspect of U_{eff} or from that of T_B/T_{IRREV}, the SMM properties of complexes **1** and **2** are clearly shown to be improved when compared with previously reported complexes **1′** and **2′**, respectively (Table S8, ESI†). Thus, the introduction of the electron-donating group in the axial ligands should be an effective route to high-performance Dy^{III}-SIM. Furthermore, the U_{eff} and T_B of complex **2** are higher than those of complex **1** by 440 K and 6 K, respectively. These significant improvements may not be related to the local symmetry of the Dy^{III} ion as the distortion of complex **2** from ideal PBP is actually larger than that of complex **1**.

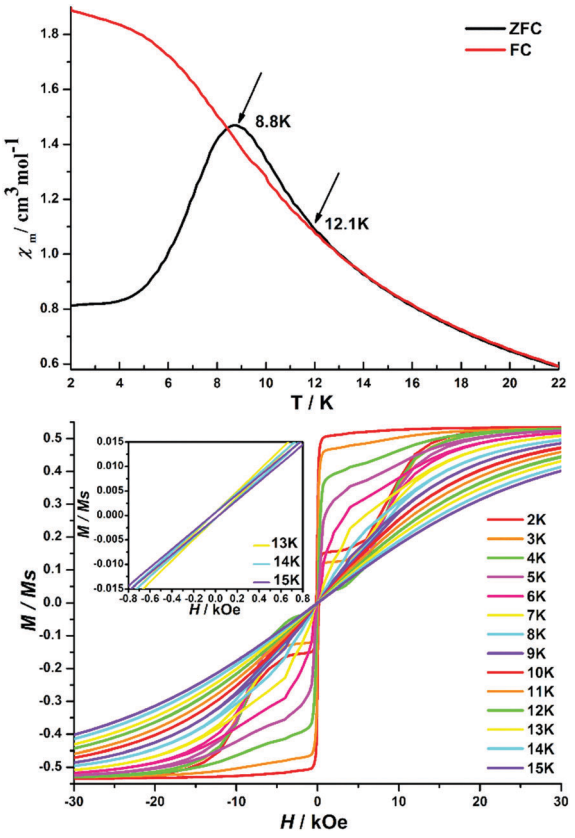

Fig. 4 Variable-field magnetization data for complex **2**, under field-cooled (FC) and zero-field-cooled (ZFC) conditions with a field of 2000 Oe (up). Magnetic hysteresis loops were measured at a sweep rate of 0.02 T s^{-1} from 2 to 15 K (down).

Theoretical analysis

For the sake of obtaining a deep understanding, *ab initio* calculations were performed for complexes **1**, **1′**, **2**, **2′** as well as **3** (Table S8, ESI†). All the g_Z values of the ground KDs of the five SIMs are calculated to be approaching the Ising limit of 20 for Dy^{III} ion (Table S6, ESI†) and thus they indicate the strong magnetic anisotropy of easy-axis type. The $g_{X,Y}/g_Z$ ratio, where g_{XY} is the averaged transversal g values, has been shown to be related to the axiality of a KD as lower ratio represents higher axiality.[12] As shown in Fig. 5, the $g_{X,Y}/g_Z$ ratios of the five SIMs are consistent with their SMM properties in the aspects of either U_{eff} or T_{IRREV}. The averaged transition magnetic moment within a given KD, μ_{QTM}, could be used to measure the strength of the corresponding QTM.[10] The μ_{QTM} of the ground KDs are also consistent with the SMM properties of the five complexes as smaller μ_{QTM} does relate with higher U_{eff} or T_{IRREV}. Furthermore, theoretical results indicate that the magnetic relaxation of complex **2** occurs *via* the third excited KD of which the energy (1179 K) is quite

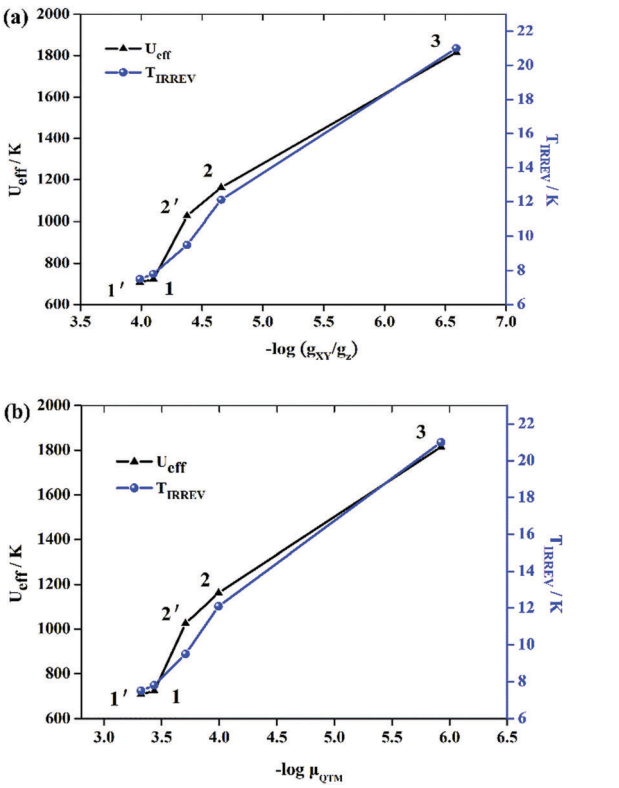

Fig. 5 $-\log(g_{XY}/g_Z)$ *vs.* U_{eff}, T_{IRREV} (up) and $-\log \mu_{QTM}$ *vs.* U_{eff}, T_{IRREV} (down), for complexes **1′**, **1**, **2′**, **2** and **3**.

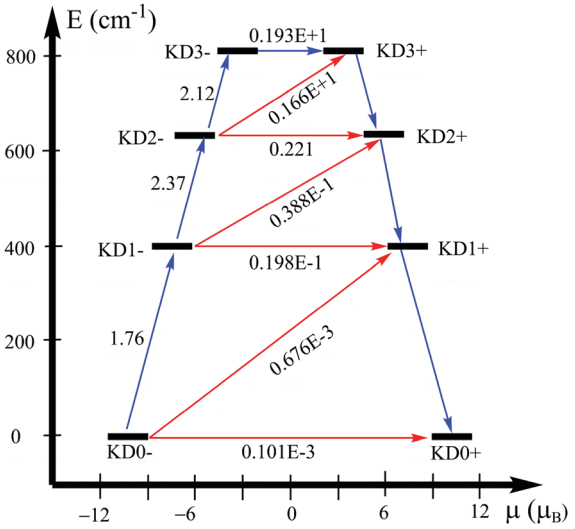

Fig. 6 Magnetization blocking barrier in complex **2**. Exchange states are arranged according to the values of their magnetic moments (bold horizontal black lines). Arrows show the transition between the states, while the numbers above the arrows are the corresponding average matrix element of the magnetic moment ($\bar{\mu}$). The relaxation pathway is outlined by arrows containing the largest $\bar{\mu}$ (blue arrows).

close to the experimental U_{eff} (1162 K) (Fig. 6 and Fig. S24, ESI†). Therefore, the *ab initio* results here should be reliable and they demonstrate that the difference in the electronic structures of the five SIMs should be the reason for their different SMM properties.

With the calculated atomic charge, the electrostatic potential (ESP) felt by the central Dy^{III} could be approximated as the sum of contributions from two axial O atoms, ESP(ax), and those from five equatorial atoms, ESP(equ). The lower the ratio ESP(equ)/ESP(ax) is, the larger the excess of axial electrostatic repulsion over that from the equatorial ligands should be. This ration is calculated to be 0.843, 0.834, 0.807, 0.789 and 0.561 for complexes **1**, **1′**, **2**, **2′** and **3**, respectively (Table 1). All these ratios are significantly lower than one, which means the apparent excess of axial repulsion felt by the central Dy^{III}. This is consistent with the fact that all these five complexes are zero-field SIM of high U_{eff}. More importantly, the ESP(equ)/ESP(ax) ratio also accounts for the difference of the SMM properties among these five complexes as clearly monotonic relation exists between this ration and either U_{eff}/T_{IRREV} or *ab initio* parameter (Fig. 7 and Fig. S26–S30, ESI†). Thus, ESP(equ)/ESP(ax) should be a useful parameter for the prediction of SMM properties of PBP mononuclear Dy^{III} complex.

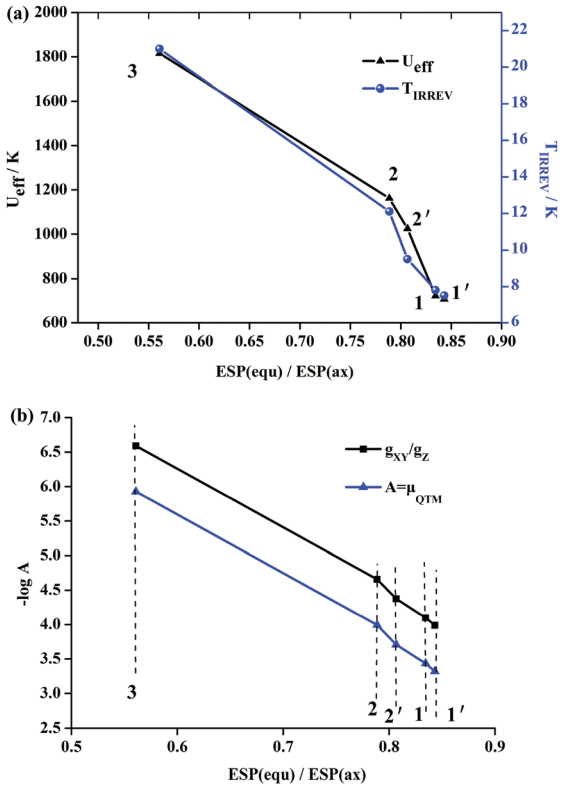

Fig. 7 ESP(equ)/ESP(ax) *vs.* U_{eff}, T_{IRREV} (up) and $-\log A$ (down) for complexes **1′**, **1**, **2′**, **2** and **3**.

The decrease of ESP(equ)/ESP(ax) ratio from complex **2′** to complex **2** arises from the increase of the magnitude of ESP(ax) (0.83 a.u. for complex **2′** *vs.* 0.85 a.u. for complex **2**) since the ESP(equ) nearly remains to be 0.67 a.u. Therefore, the ESP results do verify the importance of introducing electron-donating group in the axial ligand. A similar situation also occurs from complex **1′** to complex **1**. In the comparison between complex **1** and complex **2**, the lower ESP(equ)/ESP(ax) ratio of complex **2** could be mainly attributed to the decrease of the equatorial ESP contributions from Cl (0.28 a.u.) to Br (0.24 a.u.). Although the introduction of equatorial Br instead of Cl will lead to larger deviation from ideal PBP, the longer Dy–Br distance, as well as lower magnitude of the negative charge of Br, will reduce ESP(equ) a lot and then lead to significant increase of the axiality as well as SMM properties of **2**. Above all, the excess of axial electrostatic repulsion over the equatorial one should be a useful guide for the design of high-performance PBP Dy^{III}-SIMs.

Table 1 Results of preliminary ESP (in a.u.) analysis of complexes **1′**, **1**, **2′**, **2** and **3**

Complex	**1′**	**1**	**2′**	**2**	**3**
ESP(equ)/ESP(ax)	0.843104	0.834454	0.806634	0.788671	0.560832
ESP(equ_N)/ESP(ax)	0.513158	0.503873	0.515078	0.499460	—
ESP(equ_X)/ESP(ax)	0.329950	0.330581	0.2915556	0.2892119	—
ESP(ax)	−0.8286017	−0.8387386	−0.8315977	−0.8473232	−1.0174944
ESP(equ)	−0.6985974	−0.699889	−0.6707952	−0.6682597	−0.5706429
ESP(equ_N)	−0.425204	−0.422618	−0.428338	−0.423204	—
ESP(equ_X)	−0.273394	−0.277271	−0.242457	−0.245056	—

It is highly worthy of denoting that, both the *ab initio* parameters and ESP analysis of **3** are consistent with the corresponding experimental observations (Fig. 7 and Fig. S26–S32, ESI†). That is to say, a high excess of axial electrostatic repulsion is also achieved in **3**. The local geometry of **3**, being clearly different from the other four Dy^{III}-SIMs, is quite close to the ideal PBP geometry of D_{5h} (Table S4, ESI†). Thus, the design strategy from the aspect of ESP is not incompatible with the strategy based on symmetry and we think these two strategies are actually consistent with each other.

Conclusions

In summary, using the strategy of pursuing a high excess of axial electrostatic repulsion, two high-performance PBP Dy^{III}-SIMs were synthesized and characterized. The importance of this strategy is further verified by *ab initio* calculations and ESP analysis. This strategy is effective for both clearly distorted and nearly ideal PBP geometries and it should play an important role in the design of high-performance PBP Dy^{III}-SIMs. Beyond that, in an effort to verify the favourable SIM properties observed in this system, and encouraged by *ab initio* predictions, various groups (H_2bbpen, containing electron-donating ($-OCH_3$, $-C(CH_3)_3$) in the 4-position of the phenol rings) have pursued the use of ligands with even more high-performance PBP Dy^{III}-SIMs is ongoing in our groups.

Conflicts of interest

There are no conflicts to declare.

Acknowledgements

We gratefully acknowledge financial support from the National Natural Science Foundation of China (grant no. 21673180, 21373162, 21673181, 21727805, 21473135 and 21103137).

Notes and references

1 (*a*) R. Sessoli, D. Gatteschi, A. Caneschi and M. A. Novak, *Nature*, 1993, **365**, 141; (*b*) A. Caneschi, D. Gatteschi, R. Sessoli, A. L. Barra, L. C. Brunel and M. Guillot, *J. Am. Chem. Soc.*, 1991, **113**, 5873; (*c*) D. Gateschi, R. Sessoli and J. Villain, *Molecular Nanomagnets*, Oxford University Press, Oxford, 2006; (*d*) S. Thiele, F. Balestro, R. Ballou, S. Klyatskaya, M. Ruben and W. Wernsdorfer, *Science*, 2014, **344**, 1135; (*e*) M. Atanasov, D. Aravena, E. Suturina, E. Bill, D. Maganas and F. Neese, *Coord. Chem. Rev.*, 2015, **289–290**, 177; (*f*) J. J. Baldov, S. Cardona-Serra, A. Gaita-AriÇo and E. Coronado, *Adv. Inorg. Chem.*, 2017, **69**, 213; (*g*) S. Demir, J. M. Zadrozny and J. R. Long, *Chem. – Eur. J.*, 2014, **20**, 9524; (*h*) K. S. Pedersen, J. Bendix and R. Clérac, *Chem. Commun.*, 2014, **50**, 4396; (*i*) S. T. Liddle and J. van Slageren, *Chem. Soc. Rev.*, 2015, **44**, 6655.

2 M. N. Leuenberger and D. Loss, *Nature*, 2001, **410**, 789.

3 L. Bogani and W. Wernsdorfer, *Nat. Mater.*, 2008, **7**, 179.

4 M. Mannini, F. Pineider, P. Sainctavit, C. Danieli, E. Otero, C. Sciancalepore, A. M. Talarico, M.-A. Arrio, A. Cornia, D. Gatteschi and R. Sessoli, *Nat. Mater.*, 2009, **8**, 194.

5 (*a*) G. A. Craig and M. Murrie, *Chem. Soc. Rev.*, 2015, **44**, 2135; (*b*) J. M. Frost, K. L. M. Harriman and M. Murugesu, *Chem. Sci.*, 2016, **7**, 2470; (*c*) J. Liu, Y.-C. Chen, J.-L. Liu, V. Vieru, L. Ungur, J.-H. Jia, L. F. Chibotaru, Y. Lan, W. Wernsdorfer, S. Gao, X.-M. Chen and M.-L. Tong, *J. Am. Chem. Soc.*, 2016, **138**, 5441; (*d*) Y.-C. Chen, J.-L. Liu, L. Ungur, J. Liu, Q.-W. Li, L.-F. Wang, Z.-P. Ni, L. F. Chibotaru, X.-M. Chen and M.-L. Tong, *J. Am. Chem. Soc.*, 2016, **138**, 2829; (*e*) Y.-S. Ding, N. F. Chilton, R. E. P. Winpenny and Y.-Z. Zheng, *Angew. Chem., Int. Ed.*, 2016, **128**, 16305; (*f*) F.-S. Guo, B. M. Day, Y.-C. Chen, M.-L. Tong, A. Mansikkamäki and R. A. Layfield, *Angew. Chem., Int. Ed.*, 2017, **56**, 11445; (*g*) C. A. P. Goodwin, F. Ortu, D. Reta, N. F. Chilton and D. P. Mills, *Nature*, 2017, **548**, 439; (*h*) S. K. Gupta, T. Rajeshkumar, G. Rajaraman and R. Murugavel, *Chem. Sci.*, 2016, **7**, 5181.

6 (*a*) M. Li, H.-P. Wu, Q. Yang, H.-S. Ke, B. Yin, Q. Shi, W.-Y. Wang, Q. Wei, G. Xie and S.-P. Chen, *Chem. – Eur. J.*, 2017, **23**, 1; (*b*) M. W. Willer, J. R. Long, C. C. McLauchlan and R. H. Holm, *Inorg. Chem.*, 1998, **37**, 328.

7 L. Ungur and L. F. Chibotaru, *Inorg. Chem.*, 2016, **55**, 10043.

8 S. G. McAdams, A.-M. Ariciu, A. K. Kostopoulos, J. P. S. Walsh and F. Tuna, *Coord. Chem. Rev.*, 2017, **346**, 216.

9 J. D. Rinehart and J. R. Long, *Chem. Sci.*, 2011, **2**, 2078.

10 R. Orbach, *Proc. R. Soc. London, Ser. A*, 1961, **264**, 458.

11 K. N. Shrivastava, *Phys. Status Solidi B*, 1983, **117**, 437.

12 D. Casanova, M. Llunell, P. Alemany and S. Alvarez, *Chem. – Eur. J.*, 2005, **11**, 1479.

13 (*a*) *Bruker, SMART, SAINT, and XPREP: Area Detector Control and Data Integration and Reduction Software*, Bruker Analytical X-ray Instruments Inc., Madison, WI, 1995; (*b*) G. M. Sheldrick, *SADABS, Program for Empirical Absorption Correction*, University of Göttingen, Göttingen, 1996.

14 J. G. M. Sheldrick, *Acta Crystallogr., Sect. A: Found. Crystallogr.*, 2008, **64**, 112.

15 O. V. Dolomanov, L. J. Bourhis, R. J. Gildea, J. A. K. Howard and H. Puschmann, *J. Appl. Crystallogr.*, 2009, **42**, 339.

16 (*a*) J. Luzon and R. Sessoli, *Dalton Trans.*, 2012, **41**, 13556; (*b*) L. F. Chibotaru, *Struct. Bonding*, 2015, **164**, 185; (*c*) A. Abragam and B. Bleaney, *Electron Paramagnetic Resonance of Transition Ions*, Clarendon Press, Oxford, 1970; (*d*) D. Aravena and E. Ruiz, *Inorg. Chem.*, 2013, **52**, 13770; (*e*) J. M. Frost, K. L. M. Harriman and M. Murugesu, *Chem. Sci.*, 2016, **7**, 2470; (*f*) Y. F. Deng, T. Han, B. Yin and Y. Z. Zheng, *Inorg. Chem. Front.*, 2017, **4**, 1141.

17 (*a*) B. O. Roos, P. R. Taylor and P. E. M. Siegbahn, *Chem. Phys.*, 1980, **48**, 157; (*b*) F. Aquilante, J. Autschbach, R. K. Carlson, L. F. Chibotaru, M. G. Delcey, L. De Vico, I. F. Galvan, N. Ferre, L. M. Frutos, L. Gagliardi, M. Garavelli, A. Giussani, C. E. Hoyer, G. Li Manni, H. Lischka, D. Ma, P. A. Malmqvist, T. Muller, A. Nenov, M. Olivucci, T. B. Pedersen, D. Peng, F. Plasser, B. Pritchard, M. Reiher, I. Rivalta, I. Schapiro, J. Segarra-Marti, M. Stenrup,

D. G. Truhlar, L. Ungur, A. Valentini, S. Vancoillie, V. Veryazov, V. P. Vysotskiy, O. Weingart, F. Zapata and R. Lindh, *J. Comput. Chem.*, 2016, **37**, 506; (*c*) P. A. Malmqvist, B. O. Roos and B. Schimmelpfennig, *Chem. Phys. Lett.*, 2002, **357**, 230; (*d*) B. O. Roos, R. Lindh, P. A. Malmqvist, V. Veryazov and P. O. Widmark, *J. Phys. Chem. A*, 2004, **108**, 2851; (*e*) B. O. Roos, R. Lindh, P. A. Malmqvist, V. Veryazov and P. O. Widmark, *J. Phys. Chem. A*, 2005, **109**, 6575.

18 (*a*) L. F. Chibotaru and L. Ungur, *J. Chem. Phys.*, 2012, **137**, 064112; (*b*) L. F. Chibotaru, *Adv. Chem. Phys.*, 2013, **153**, 397.